ADVANCED MATERIALS
www.advmat.de

Linear Electro-Optic Modulation in Highly Polarizable Organic Perovskites

*Meng-Jia Sun, Chao Zheng, Yuan Gao, Andrew Johnston, Amin Morteza Najarian, Pei-Xi Wang, Oleksandr Voznyy, Sjoerd Hoogland, and Edward H. Sargent**

Electrical-to-optical signal conversion is widely employed in information technology and is implemented using on-chip optical modulators. State-of-the-art modulator technologies are incompatible with silicon manufacturing techniques: inorganic nonlinear crystals such as $LiNbO_3$ are integrated with silicon photonic chips only using complex approaches, and hybrid silicon–$LiNbO_3$ optical modulators show either low bandwidth or high operating voltage. Organic perovskites are solution-processed materials readily integrated with silicon photonics; and organic molecules embedded within the perovskite scaffold allow in principle for high polarizability. However, it is found that the large molecules required for high polarizability also require an increase of the size of the perovskite cavity: specifically, using the highly polarizable DR^{2+} (R = H, F, Cl) in the A site necessitates the exploration of new X-site options. Only by introducing BF_4^- as the X-site molecule is it possible to synthesize $(DCl)(NH_4)(BF_4)_3$, a material exhibiting a linear EO coefficient of 20 pm V^{-1}, which is 10 times higher than that of metal halide perovskites and is a 1.5 fold enhancement compared to reported organic perovskites. The EO response of the organic perovskite approaches that of $LiNbO_3$ ($r_{eff} \approx 30$ pm V^{-1}) and highlights the promise of rationally designed organic perovskites for use in efficient EO modulators.

In silicon photonics, the conversion of information from the electrical to the optical domain is realized using on-chip light modulators.[1] These devices rely on silicon p–n-junctions which modulate the phase of the light under an applied field. Impressive multi-GHz information processing speeds are realized; but the devices require large footprints in light of the weak interaction of light with silicon free carriers.

The linear EO effect, also known as the Pockels effect, relies on noncentrosymmetric crystals whose spontaneous polarization is modulated using an electric field to cause a change in refractive index.[2] Inorganic EO-active crystals are typically based on perovskite oxides, such as lithium niobite and barium titanate,[3] but their integration is a challenge with silicon photonics chips.[4] Organic nonlinear chromophores exhibit tunable polarized pi-scaffolds, which result in large changes in refractive index at high modulation speeds,[5] and are solution-processed and compatible with silicon; however, they often suffer a loss of polarization in the solid state due to the formation of centrosymmetric crystal packing caused by dipole–dipole interactions.[6] Although the noncentrosymmetric orientation of organic chromophores can be realized by poling at elevated temperature, in many case, the macroscopic nonlinear susceptibilities fell short of expectations due to the disorientation of molecules in low temperature.[5c]

Organic perovskites are a class of perovskite materials with the general formula ABX_3 in which the A and B sites are occupied by organic cations and the X site is a monovalent nonmetallic counterion (**Figure 1**a). The 3D network is composed of corner-sharing BX_6 octahedra connected via noncovalent interactions with the A site occupying the octahedral cavities.[7] This materials system offers a means to construct noncentrosymmetric structures by molecular engineering of organic components.[8] We recently showed EO modulation from an organic perovskite: this material, $(DH)(NH_4)I_3$, had *N*-methyl-*N*′-diazabicyclo[2.2.2]octonium in the A-site, and this resulted in the noncentrosymmetry of the crystal.[9]

Spontaneous polarization (P_s)—a key consideration for determining the strength of the EO effect—depends on the dipole moment of the A site and its alignment in the cavity of the BX_6 frameworks.[10] Additionally, the noncovalent interactions between the A- and X-site constituents distort the BX_6 octahedra and induce structural asymmetry, resulting in polarization. As a result, increasing the dipole moment of the A-site cation is a path toward increasing the total polarization in the crystal. This can be done by engineering the A-site cation with polarizable functional groups. As the size of the cavity of the BX_6 framework is finite, only certain sizes of A-site cations can fit in the 3D perovskite scaffold.

Here, we demonstrate a new class of organic perovskites which overcome the collapse of the 3D perovskite structure

Dr. M.-J. Sun, Dr. C. Zheng, Dr. Y. Gao, A. Johnston, Dr. A. M. Najarian, Dr. P.-X. Wang, Dr. S. Hoogland, Prof. E. H. Sargent
Department of Electrical and Computer Engineering
University of Toronto
10 King's College Road, Toronto, Ontario M5S 3G4, Canada
E-mail: ted.sargent@utoronto.ca
Prof. O. Voznyy
Department of Physical and Environmental Sciences
University of Toronto, Scarborough
1065 Military Trail, Toronto, Ontario M1C 1A4, Canada
The ORCID identification number(s) for the author(s) of this article can be found under https://doi.org/10.1002/adma.202006368.

DOI: 10.1002/adma.202006368

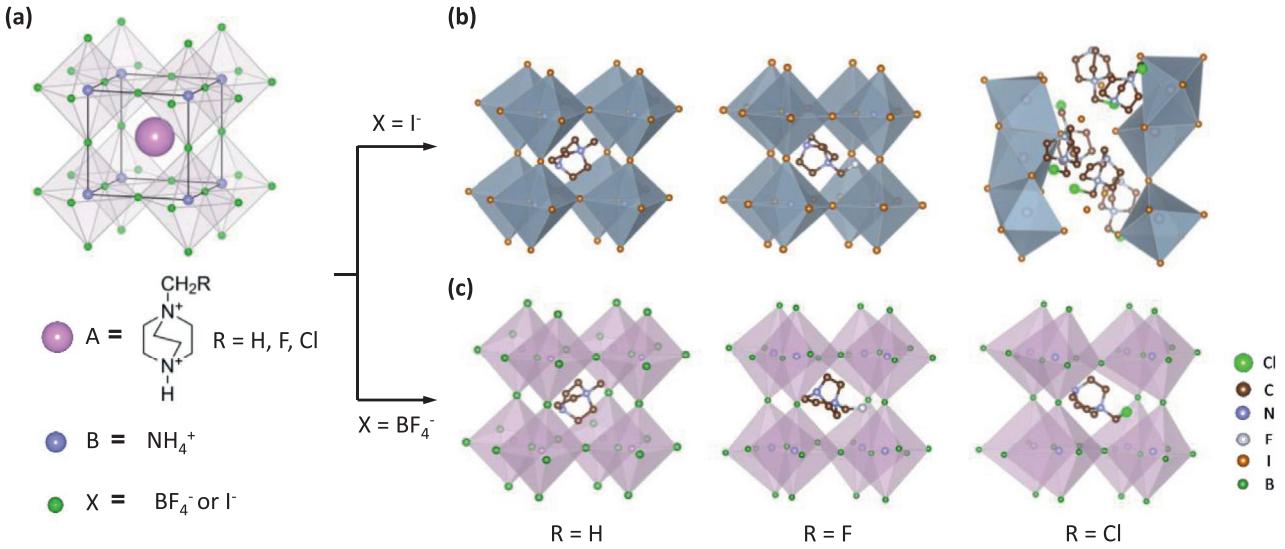

Figure 1. 3D organic perovskite design. a) Structure and composition of 3D organic perovskites. b,c) Structural evolution of the DR^{2+}-based perovskites with I^- (b) and BF_4^- (c) as X sites, respectively.

upon the addition of large A-site molecules. DR^{2+} (D = *N*-methyl-*N*′-diazabicyclo[2.2.2]octonium, R = H, F, Cl) were used as the A-site cations: we replaced one hydrogen atom on the methyl group with a larger, more polarizable halogen atom. The halogenation was realized by applying a one-step nucleophilic reaction between halomethane and *N*,*N*′-diazabicyclo[2.2.2]octonium. The larger polarizability of the halogen atoms increases the molecular dipole strength.[11]

When I^- is used as the X-site, the perovskite structure collapses when we use Cl in the A-site molecule. To prevent the collapse of the 3D framework, we used BF_4^- instead of I^- as the X site (Figure 1b). The large radius of BF_4^- (232 pm) stabilizes the 3D structure for the highly polarizable Cl-substituted cation. Each cation is isolated in BX_6 cages, which limits dipole–dipole interactions and so avoids the formation of centrosymmetric crystal packing present in other organic EO modulator materials. The structural dimension evolution is in good agreement with the Goldschmidt's Tolerance Factor (Table S1, Supporting Information).[12] With the BF_4^- as the X-site counterion, we were able to create three new 3D organic perovskites with a general formula of $(DR)(NH_4)(BF_4)_3$ (Figure 1c).

Each of the crystals displayed in Figure 1 was prepared in an aqueous solution through a step-cooling method (see the Experimental Section) and their structures were determined by powder- and single-crystal X-ray diffraction (**Figure 2** and Figures S2–S4 and Table S2, Supporting Information). As seen in Figure 2a, $(DCl)(NH_4)(BF_4)_3$ displays a typical 3D perovskite structure, composed of a corner-sharing network of $(NH_4)(BF_4)_6$ octahedra with a DCl^{2+} cation occupying the octahedral cavities and maintaining the electroneutrality of the system. All components are held together by hydrogen and halogen bonds. The DCl^{2+} is closely linked to the $(NH_4)(BF_4)_6$ octahedra via C—H···F hydrogen bonds (2.31–2.60 Å, red dotted line) and C—Cl···F heterohalogen···halogen interactions (3.72 Å, blue dotted line), which align the cation in each cavity (Figure 2b). The octahedron formed between NH_4^+ and BF_4^- by N—H···F hydrogen bonds (2.19–2.58 Å, red dotted line) shows a distorted geometry (Figure 2c). The noncovalent bonding decreases the rigidity of the octahedra, facilitating a distortion large enough to allow the DCl^{2+} to fit inside the perovskite cavity (Figure S5 and Table S3, Supporting Information).[13] The degree of the distortion in $(DCl)(NH_4)(BF_4)_3$ is an order of magnitude larger than in the H and F counterparts, which we attribute to the size of DCl^{2+} cation.

We also investigated the phase purity with powder X-ray diffraction: the experimental and simulated powder X-ray diffraction were well-matched, which confirms that the crystal is in a single phase (Figure 2d). Strong second harmonic generation (SHG) signal was observed at room temperature when the crystal powder was illuminated with a 1030 nm femtosecond laser, confirming the noncentrosymmetric structure of the crystal and its propensity for second-order optical nonlinearity (Figure 2e). Under the same experimental conditions, the SHG intensity of $(DCl)_2(NH_4)_3I_7$ was several orders of magnitude lower. As SHG is primarily a result of the polarized electrons in the material, we can conclude that the polarization is significantly stronger in the $(DCl)(NH_4)(BF_4)_3$ materials compared to their I^- counterpart.

We used density functional theory to investigate the macroscopic polarization P_s in the organic perovskite crystals. The P_s depends primarily on the dipole ordering of the A-sites.[8,10a] We first calculated the molecular dipole moments and electrostatic potential maps of the A-site molecules (**Figure 3**a–c). The dipole of DH^{2+} has a strength of ≈1.69 D and is oriented along the molecular trifold axis. This dipole originates from the reduction of the molecular symmetry through the attachment of the methyl group on the *N*,*N*′-diazabicyclo[2.2.2]octonium core. When one H atom on DH^{2+} is replaced by a halogen atom (F and Cl), the dipole moments increase to 5.49 D for DF^{2+} and 8.17 D for DCl^{2+} (Figure 3a-c, left). This increase is a direct consequence of the increased electronegativity of F and Cl. The increase in dipole moments is evident from the electrostatic potential mapping shown in Figure 3a-c. The halogenation redistributes the electron density to make the rest of the

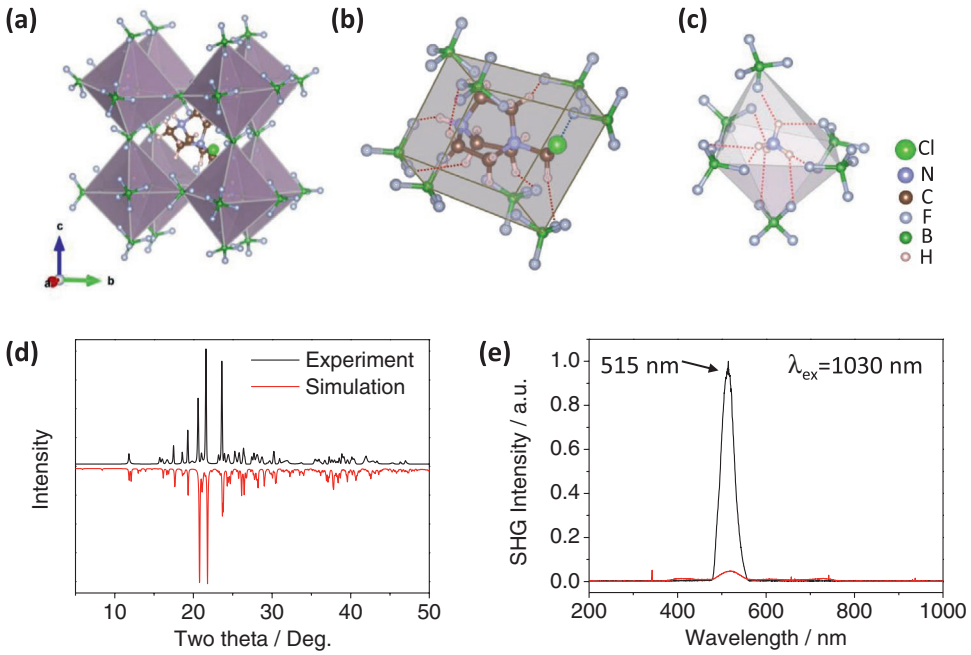

Figure 2. Crystal properties of $(DCl)(NH_4)(BF_4)_3$. a) 3D single-crystal packing. b) Hydrogen and halogen bonding in the cavity between DCl^{2+} and BF_4^-. c) Hydrogen bonding in the octahedra between NH_4^+ and BF_4^-. d) The experimental and simulated X-ray diffraction patterns for $(DCl)(NH_4)(BF_4)_3$. e) SHG signal from $(DCl)(NH_4)(BF_4)_3$ (black line) and $(DCl)_2(NH_4)_3I_7$ (red line) crystal powders.

molecule more positive and the halogen side electronegative. We calculated the P_s of the three $(DR)(NH_4)(BF_4)_3$ crystals using the Berry phase polarization method based on the single-crystal XRD data. It revealed that the electron redistribution leads to a dipole direction off-axis by ~15° with respect to the trifold axis of the *N,N′*-diazabicyclo[2.2.2]octonium core. As shown in Figure 3f, $(DCl)(NH_4)(BF_4)_3$ exhibits the largest P_s due to an optimal alignment of the large molecular dipole of DCl^{2+} in the 3D noncentrosymmetric structure. The DCl^{2+} molecule is aligned in the same orientation along the b axis of the 3D structure, giving rise to an overall polarization (Figure S6c, Supporting Information). The crystal of $(DF)(NH_4)(BF_4)_3$, exhibits the smallest P_s among the three cations (Figure 3e), because the DF^{2+} cations are packed antiparallelly, resulting in a centrosymmetric crystal structure and a cancellation of P_s (Figure S6b, Supporting Information). The different packing behavior than the Cl derivative can be ascribed to the smaller size of F and its less distorted perovskite framework, allowing the molecules

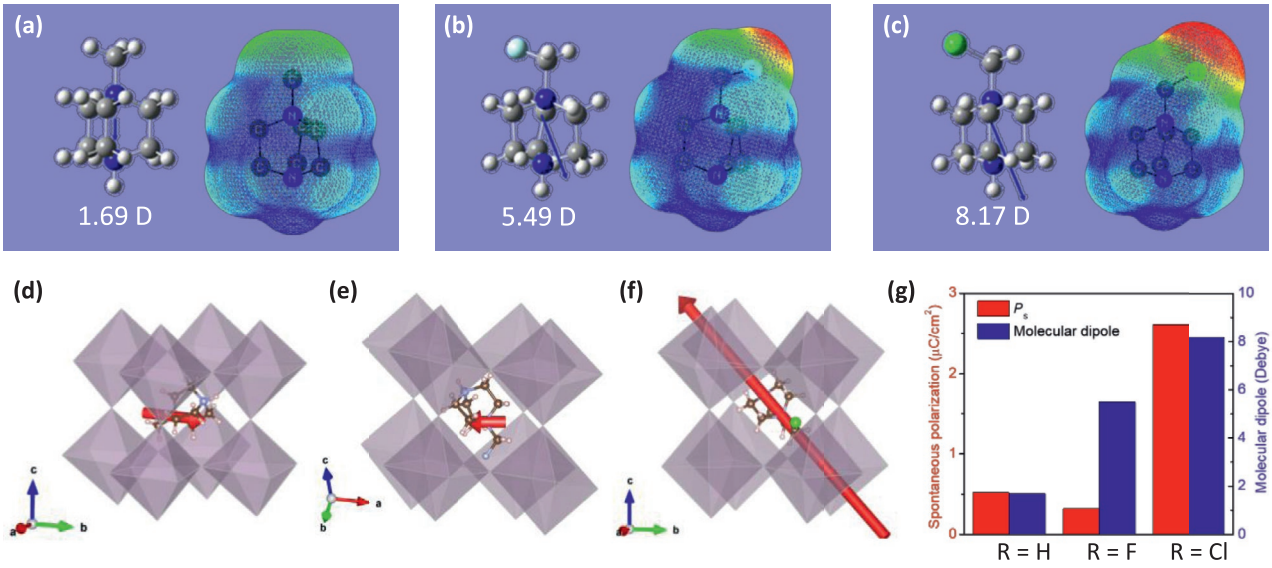

Figure 3. DFT calculations. a–c) Molecular dipole moments and electrostatic potential mapping of the DR^{2+} cation: a) R = H; b) R = F; c) R = Cl). d–f) The vector of P_s in $(DR)(NH_4)(BF_4)_3$ crystals: d) R = H; e) R = F; f) R = Cl). g) The comparison between molecular dipole moments and P_s.

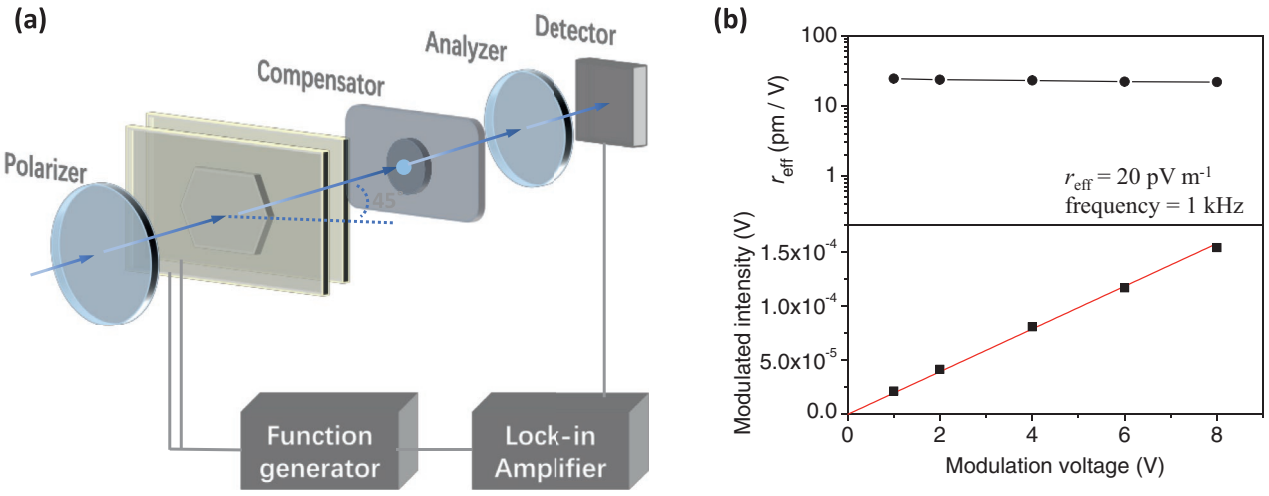

Figure 4. Linear electro-optic effect characterization. a) Schematics of the experimental setup. b) EO coefficient at different modulated voltage (top) and the linear growth of the transmitted light power increasing with the modulation voltage (bottom).

more freedom to rotate and align in an antiparallel fashion. By comparing the molecular dipole moments with the crystal P_s (Figure 3g), we found that only the combination of large molecular dipoles that were aligned in noncentrosymmetric crystal structures resulted in an improved P_s. The Cl-substituted A-site cation material could form a low-dimensional structure when I^- was used as the X-site ($(DCl)_2(NH_4)_3I_7$). However, we found the polarization to be very small (Figure S6d, Supporting Information), due to the undesirable molecular orientation that results in a cancellation of the dipoles. The direction and the coordinates of P_s in the unit cells of the crystals are summarized in Figure S6 and Table S4 in Supporting Information.

The linear EO effect is characterized by measuring the polarization change of a laser beam transmitted through the crystal as a function of applied electric field. The EO effect is given by the linear change of the refractive index with an applied electric field, E, expressed:

$$\Delta n = \frac{1}{2} r_e n^3 E \tag{1}$$

where r_e is the effective EO coefficient when an electric field is applied. The EO coefficient of $(DCl)(NH_4)(BF_4)_3$ was determined quantitatively at the standard telecom wavelength of 1550 nm using the modified Teng–Man technique.[14] A schematic of the experimental setup used is shown in **Figure 4a**. Briefly, a laser beam at 1550 nm was passed through a linear polarizer to the crystal surface at an angle 45°, so that the parallel and perpendicular components of the optical field are equal in amplitude. The crystal was sandwiched between a pair of ITO electrodes to which an electric field was applied to induce the refractive index change for the light passing through the crystal. The transmitted beam was sent through a Soleil-Babinet compensator and an analyzer and finally into a Ge near-infrared photodetector connected to a lock-in amplifier. The applied electrical field was modulated by a peak-to-peak voltage (V_{pp}) of 10 V (electric field strength, $E = 5 \times 10^3$ V m^{-1}) at a frequency of 1 kHz. The power of the transmitted light increased linearly as a function of the applied AC voltage (Figure 4b, bottom), which confirms the linear EO effect rules out the quadratic Kerr effect. The linear EO coefficient of r_{eff} was calculated with the following equation:[14]

$$r_{eff} = \frac{\lambda I_{ac}}{\pi V_{ac} I_c n^2} \frac{\left(n^2 - \sin^2\theta\right)^{3/2}}{\left(n^2 - 2\sin^2\theta\right)} \frac{1}{\sin^2\theta} \tag{2}$$

where $\theta = 45°$, $V_{ac} = V_{pp} \sin\theta$, I_{ac} is the amplitude of the modulated light intensity and I_c is the half intensity of the maximum intensity of the output laser at the detector. Using this method we found that the EO coefficient was 20 pm V^{-1} at 1 kHz and was independent of the operating voltage (Figure 4b, top), which means that this EO process is second-order nonlinearly. This EO coefficient is higher than that of layered hybrid perovskites[2c] and is comparable to conventional nonlinear crystals.[1a,15] In contrast, the linear EO effect of $(DH)(NH_4)(BF_4)_3$ and $(DCl)_2(NH_4)_3I_7$ crystals were too weak to detect due to the small P_s.

In summary, we report highly polarizable organic perovskites by introducing halogen functional groups in the A-site cation. We demonstrated that the $(DCl)(NH_4)(BF_4)_3$ crystal exhibits a strong linear EO effect with an effective EO coefficient of 20 pm V^{-1}. By combining experimentally determined crystallographic information with DFT simulations, we showed that the large EO response originates from the ability of the crystal to align large molecular dipoles within the 3D perovskite structure. These findings highlight the potential of rationally designed all-organic perovskites for use in on-chip modulators.

Experimental Section

Material Synthesis: DR^{2+} (R = H, F, Cl) cations were synthesized and characterized according to the patent.[16] Briefly, *N*,*N*′-diazabicyclo[2.2.2]octonium and methyl iodide were dissolved in acetone

in a 1:1.1 mole ratio at room temperature, then the mixed solution was stabilized in the dark for 48 h. The resulting precipitate was collected by filtration and washed with a large amount of diethyl ether to afford high-yield (DH)I as transparent crystals. (DF)I and (DCl)Cl were prepared using the similar method by reacting *N*,*N*′-diazabicyclo[2.2.2]octonium with fluoroiodomethane and dichloromethane, respectively. The (DR)$(NH_4)(BF_4)_3$ crystals were prepared by adopting the step-cooling method by mixing stoichiometric amounts of DR and NH_4BF_4 in excess HBF_4 aqueous solution in a 20 mL vial. The mixture was dissolved by heating it up to 80 °C for 1h. The clear solution was then cooled to room temperature at a rate of 4 K h^{-1} to yield centimeter-sized transparent crystals. The crystals of I^- counterpart were prepared in a similar way, by using HI solution instead of HBF_4 aqueous solution.

Single-Crystal X-ray Analysis: Single-crystal structures were measured with Bruker Kappa APEX-DUO diffractometer equipped with a rotating anode with graphite-monochromated Mo-Kα radiation (Burker Triumph, λ = 0.71073Å). The structures were solved by SHLEXT and SHELXL-2016/6, respectively. The detailed crystal information was listed in Table S2 (Supporting Information).

Second Harmonic Generation (SHG) Measurement: The crystals of $(DCl)(NH_4)(BF_4)_3$ and $(DCl)_2(NH_4)_3I_7$ were ground into powders comprising particles of average size 100 µm. The thicknesses of the two samples were kept at approximately 500 µm. The powders were illuminated using a 1030 nm laser. After the collected signal was passed through an 800 nm short-pass filter, signal was collected using a spectrometer having detection range from 200 to 1000 nm.

Density Functional Theory: The molecular dipole moments of DR^{2+} cations were calculated by DFT calculation carried out in Gaussian09 package using the B3LYP functional. The electronic structures were optimized using 6-31G basis set. The crystal polarization calculations were performed in the framework of DFT[17] with Perdew-Burke-Ernzerhof generalized gradient approximation[18] (GGA-PBE) for the exchange-correlation functional and GTH pseudopotentials.[19] Van der Waals correction is considered for all calculations at a DFT-D3 level.[20] The polarization calculations were performed using CP2K.[21] An energy cutoff of 600 Ry was set for Gaussian basis sets with auxiliary planewave method. Geometry optimization was performed under BFGS algorithm. Berry phase approach was utilized to calculate system electric polarization.[22]

[CCDC 2006695–2006698 contains the supplementary crystallographic data for this paper. These data can be obtained free of charge from The Cambridge Crystallographic Data Centre via www.ccdc.cam.ac.uk/data_request/cif.]

Supporting Information

Supporting Information is available from the Wiley Online Library or from the author.

Acknowledgements

This work was financially supported by Huawei Technologies Canada Co., Ltd. and the Natural Sciences and Engineering Research Council (NSERC). Computations were performed on the Niagara supercomputer at the SciNet HPC Consortium. SciNet is funded by: the Canada Foundation for Innovation; the Government of Ontario; Ontario Research Fund – Research Excellence; and the University of Toronto. The authors thank Dr. Alan J. Lough (Department of Chemistry, University of Toronto) for the single-crystal X-ray diffraction analysis.

Conflict of Interest

The authors declare no conflict of interest.

Keywords

electro-optics, noncentrosymmetry, optical nonlinearity, organic perovskites, polarization

Received: September 17, 2020
Revised: November 20, 2020
Published online:

[1] a) E. L. Wooten, K. M. Kissa, A. Yi-Yan, E. J. Murphy, D. A. Lafaw, P. F. Hallemeier, D. Maack, D. V. Attanasio, D. J. Fritz, G. J. McBrien, D. E. Bossi, *IEEE J. Sel. Top. Quantum Electron.* **2000**, *6*, 69; b) I. S. Amiri, S. R. B. Azzuhri, M. A. Jalil, H. M. Hairi, J. Ali, M. Bunruangses, P. Yupapin, *Micromachines* **2018**, *9*, 452.

[2] a) C. Wang, M. Zhang, X. Chen, M. Bertrand, A. S. Ansari, S. Chandrasekhar, P. Winzer, M. M. Lončar, *Nature* **2018**, *562*, 101; b) A. D. Dupuy, Y. Kodera, J. E. Garay, *Adv. Mater.* **2016**, *28*, 7970; c) Y. Gao, G. Walters, Y. Qin, B. Chen, Y. Min, A. Seifitokaldani, B. Sun, P. Todorovic, M. I. Saidaminov, A. Lough, S. Tongay, S. Hoogland, E. H. Sargent, *Adv. Mater.* **2019**, *31*, 1808336.

[3] a) R. S. Weis, T. K. Gaylord, *Appl. Phys. A* **1985**, *37*, 191; b) S. Abel, F. Eltes, J. E. Ortmann, A. Messner, P. Castera, T. Wagner, D. Urbonas, A. Rosa, A. M. Gutierrez, D. Tulli, P. Ma, B. Baeuerle, A. Josten, W. Heni, D. Caimi, L. Czornomaz, A. A. Demkov, J. Leuthold, P. Sanchis, J. Fompeyrine, *Nat. Mater.* **2019**, *18*, 42.

[4] a) S. Abel, T. Stöferle, C. Marchiori, C. Rossel, M. D. Rossell, R. Erni, D. Caimi, M. Sousa, A. Chelnokov, B. J. Offrein, J. Fompeyrine, *Nat. Commun.* **2013**, *4*, 1671; b) L. Chen, R. M. Reano, *Opt. Express* **2012**, *20*, 4032.

[5] a) S. R. Marder, L.-T. Cheng, B. G. Tiemann, A. C. Friedli, M. Blanchard-Desce, J. W. Perry, J. Skindhøj, *Science* **1994**, *263*, 511; b) L. R. Dalton, *J. Phys.: Condens. Matter* **2003**, *15*, R897; c) S. R. Marder, B. Kippelen, A. K.-Y. Jen, N. Peyghambarian, *Nature* **1997**, *388*, 845.

[6] L. R. Dalton, A. W. Harper, B. H. Robinson, *Proc. Natl. Acad. Sci. USA* **1997**, *94*, 4842.

[7] C. A. Bremner, M. Simpson, W. T. A. Harrison, *J. Am. Chem. Soc.* **2002**, *124*, 10960.

[8] H.-Y. Ye, Y.-Y. Tang, P.-F. Li, W.-Q. Liao, J.-X. Gao, X.-N. Hua, H. Cai, P.-P. Shi, Y.-M. You, R.-G. Xiong, *Science* **2018**, *361*, 151.

[9] Y. Gao, S. M. Alsadat, A. Johnston, C. Zheng, G. Walters, Q. Feng, X. Wang, M.-J. Sun, A. M. Najarian, D. Xue, Y.-K. Wang, M. I. Saidaminov, O. Voznyy, S. Hoogland, E. H. Sargent, unpublished.

[10] a) H. Wang, H. Liu, Z. Zhang, Z. Liu, Z. Lv, T. Li, W. Ju, H. Li, X. Cai, H. Han, *npj Comput. Mater.* **2019**, *5*, 17; b) F. Wang, *Phys. Rev. B* **1999**, *59*, 9733.

[11] a) H.-Y. Zhang, Y.-Y. Tang, P.-P. Shi, R.-G. Xiong, *Acc. Chem. Res.* **2019**, *52*, 1928; b) Y. Ai, X.-G. Chen, P.-P. Shi, Y.-Y. Tang, P.-F. Li, W.-Q. Liao, R.-G. Xiong, *J. Am. Chem. Soc.* **2019**, *141*, 4474.

[12] V. M. Goldschmidt, *Naturwissenschaften* **1926**, *14*, 477.

[13] a) M. W. Lufaso, P. M. Woodward, *Acta Crystallogr., Sect. B: Struct. Sci.* **2004**, *60*, 10; b) J. Alonso, M. Martinez-Lope, M. Casais, M. Fernandez-Diaz, *Inorg. Chem.* **2000**, *39*, 917.

[14] a) C. C. Teng, H. T. Man, *Appl. Phys. Lett.* **1990**, *56*, 1734; b) Y. Shuto, M. Amano, *J. Appl. Phys.* **1995**, *77*, 4632.

[15] a) J. L. Casson, K. T. Gahagan, D. A. Scrymgeour, R. K. Jain, J. M. Robinson, V. Gopalan, R. K. Sander, *J. Opt. Soc. Am. B* **2004**, *21*, 1948; b) A. Yariv, P. Yeh, *Photonics: Optical Electronics in Modern Communications*, Oxford University Press, Oxford, UK **2007**.

[16] G. Veronique, S. Graham, (Oxford University Innovation) *UK WO2014/68341*, **2014**.

[17] W. Kohn, L. J. Sham, *Phys. Rev.* **1965**, *140*, A1133.
[18] J. P. Perdew, K. Burke, M. Ernzerhof, *Phys. Rev. Lett.* **1996**, *77*, 3865.
[19] S. Goedecker, M. Teter, J. Hutter, *Phys. Rev. B* **1996**, *54*, 1703.
[20] S. Grimme, J. Antony, S. Ehrlich, H. Krieg, *J. Chem. Phys.* **2010**, *132*, 154104.
[21] a) G. Lippert, J. Hutter, M. Parrinello, *Mol. Phys.* **1997**, *92*, 477; b) J. VandeVondele, M. Krack, F. Mohamed, M. Parrinello, T. Chassaing, J. Hutter, *Comput. Phys. Commun.* **2005**, *167*, 103; c) J. Hutter, M. Iannuzzi, F. Schiffmann, J. VandeVondele, *WIREs Comput. Mol. Sci.* **2014**, *4*, 15.
[22] S. Luber, *J. Chem. Phys.* **2014**, *141*, 234110.